Abrupt and gradual changes in neuronal processing upon falling asleep and awakening

Amit Marmelshtein[1,2*], Barak Lavy[3*], Barak Hadad[2], Yuval Nir[1,2,3,4]

1. Sagol School of Neuroscience, Tel Aviv University; Tel Aviv 6997801, Israel
2. Department of Physiology & Pharmacology, School of Medicine, Tel Aviv University, Tel Aviv 6997801, Israel
3. Department of Biomedical Engineering, Faculty of Engineering, Tel Aviv University, Tel Aviv 6997801, Israel
4. The Sieratzki-Sagol Center for Sleep Medicine, Tel Aviv Sourasky Medical Center, Tel Aviv, Israel.

*These authors contributed equally

Corresponding author: Yuval Nir, ynir@tauex.tau.ac.il

Abstract

The neural processes that change when falling asleep are only partially understood. At the cortical level, features of both spontaneous neural activity and sensory responses change between wakefulness and sleep. For example, in early auditory cortex sleep increases the occurrence of post-onset silent (OFF) periods and elevates population synchrony. However, it remains unknown whether such changes occur abruptly or gradually around sleep onset and awakening. Here, we recorded spontaneous and sound-evoked neuronal spiking activity in early auditory cortex along with polysomnography during thousands of episodes when rats fell asleep or woke up. We found that when falling asleep, stimulus-induced neuronal silent periods (OFF periods), characteristic of non-rapid eye movement (NREM) sleep, increased within few seconds around sleep onset. By contrast, a gradual increase in neuronal population synchrony built up over dozens of seconds until reaching maximal levels. EEG auditory-evoked potentials representing stimulus-triggered "K complexes" changed along with post-onset neuronal firing, whereas ongoing EEG slow wave activity was associated with neuronal population synchrony. Similar effects, but with opposite direction, were observed around awakenings. The results highlight late stimulus-induced neuronal silence as a key feature changing abruptly around transitions between vigilance states, likely reflecting neuronal bistability and manifesting also in EEG evoked potentials. More generally, these findings emphasize the added value of going beyond monitoring ongoing activity and perturbing the nervous system to reveal its state - an insight that could also help guide development of more sensitive non-invasive monitors of falling asleep in humans.

Keywords

Auditory, A1, rats, NREM, OFF periods, EEG, click-trains

Introduction

Every night we drift into sleep, becoming disconnected as our conscious experience of the sensory environment largely subsides. This profound shift in our mental state raises fascinating questions regarding the ways by which brain states shape our behavior and subjective experiences. Previous work has investigated how different brain states affect sensory processing at the neuronal level (Harris and Thiele, 2011; Lee and Dan, 2012; Mcginley et al., 2015). In the auditory domain, such research revealed how factors such as arousal, locomotion, sleep pressure, ongoing behavioral tasks, and attention influence auditory responses (Edeline et al., 2001; Issa and Wang, 2008; Atiani et al., 2009; Harris and Thiele, 2011; Nir et al., 2013; Sela et al., 2020a; Marmelshtein et al., 2023).

In a recent investigation, we examined responses to sounds within the early auditory cortex of rats across vigilant wakefulness, sleep deprivation, NREM sleep, and REM sleep. Our findings revealed robust modulation in specific aspects of neuronal activity, particularly in population synchrony and post-onset responses (Marmelshtein et al., 2023). In contrast, other features such as spontaneous firing rates only showed modest modulation, while onset responses were largely unaffected by vigilance states (Marmelshtein et al., 2023). While these changes were examined over dozens of minutes or even hours, the dramatic and relatively abrupt brain state changes accompanying sleep onset and offset offer a potentially valuable model for understanding how changes in brain states can rapidly influence behavior and perception, irrespective of confounding factors that may operate at slower time scales.

Falling asleep is a continuous and dynamic process, reflecting a progressing sequence of changes in electrical, physiological, behavioral, and phenomenological phenomena (Ogilvie, 2001; Lacaux et al., 2023) governed by diminished activity in subcortical wake-promoting circuits co-occurring with increased sleep-promoting neuromodulation (Nir and de Lecea, 2023). Changes in heart rate, blood flow, eye movements, behavioral reaction times, as well as reports of subjective experience take minutes to develop and coincide with sequential changes in electroencephalogram (EEG) activity. Such changes range from diminished alpha oscillations and increased cortical theta activity, to the occurrence of sharp-waves, and ultimately to bona-fide sleep events such as K-Complexes and sleep spindles (Hori et al., 1994; Adamantidis et al., 2019). These changes lead one to consider falling sleep as an inherently gradual and continuous process, which does not necessarily occur at any single moment (Ogilvie, 2001). On the other hand, measures of behavioral responsiveness, and possibly

some EEG phenomena, do change rapidly around sleep onset, possibly at the order of a few seconds (Ogilvie, 2001; Strauss et al., 2022). This raises the question of whether there is a functionally-relevant abrupt binary switch within the extended process of falling asleep. We sought to address this open question by testing whether changes in cortical neuronal activities accompanying sleep onset exhibit abrupt or gradual dynamics.

To date, studies examining sleep onset with high temporal resolution (seconds) were typically performed non-invasively in humans. These studies have primarily focused on aspects such as the timing and topographical changes in different EEG components and functional magnetic resonance imaging (fMRI) measurements (Hori et al., 1994; Fukunaga et al., 2006). Auditory EEG responses around sleep onset reveal that signatures of low-level auditory processing, as reflected in early EEG components or responses related to stimulus-specific adaptation, are not robustly modulated by sleep onset (Strauss et al., 2015). By contrast, measures of high-level processing such as P300, responses linked to predictive coding, and measures of baseline EEG complexity and connectivity, are strongly suppressed upon falling asleep (Strauss et al., 2015, 2022). However, non-invasive studies lack the ability to investigate processes at the neuronal level. On the other hand, studies focusing on sleep-related changes in cortical sensory responses at the neuronal level (Issa and Wang, 2008, 2011, 2013; Sela et al., 2016, 2020a; Hayat et al., 2022; Marmelshtein et al., 2023) have not investigated modulations within seconds around state transitions. In this study, we aimed to bridge this gap by investigating, with high-temporal resolution, changes in neuronal activity in the auditory cortex as rats fell asleep or woke up. Our findings reveal that post-onset silence (or firing) undergoes substantial and abrupt changes within few seconds upon falling asleep (or awakening). Other aspects of auditory processing such as elevated population synchrony, vary at a slower time scale (tens of seconds or minutes), reflecting gradual aspects of the extended sleep onset process. We also find rapid modulation in frontal EEG activity exhibiting a selective association between the EEG sound-evoked potential (likely reflecting a stimulus-induced K-complex) and the auditory cortex post-onset response, whereas baseline slow wave activity is associated with auditory cortex population synchrony.

Results

We investigated how sensory processing changes during the transitions between wakefulness and sleep by conducting sixteen experiments on adult male Wister rats (n = 6) implanted with microwire arrays targeting the auditory cortex, as well as monitoring with polysomnography including electroencephalography (EEG), electromyography (EMG), and synchronized video (Methods, Figure 1A-C). Rats were situated within a computer-controlled motorized running wheel placed inside an acoustic chamber for a total duration of 10 hours, commencing at light onset. In the first part of the experiment (5 hours), the wheel was periodically rotated for 4-7 seconds each time, alternating with idle intervals of 36-39 seconds (Figure 1D). In the second part of the experiment (recovery), rats were allowed to sleep undisturbed (while still in the wheel apparatus) for an additional 5 hours, during which they naturally transitioned between sleep and wakefulness. Throughout the entire 10h experimental period, we continuously presented auditory stimuli, 500ms-long click-trains at 2, 10, 20, 30 and 40Hz (Figure 1C) with an average inter-stimulus interval of 2s, played from an overhead free-field speaker (Methods) so that many of these sounds occurred around episodes of falling asleep or awakenings.

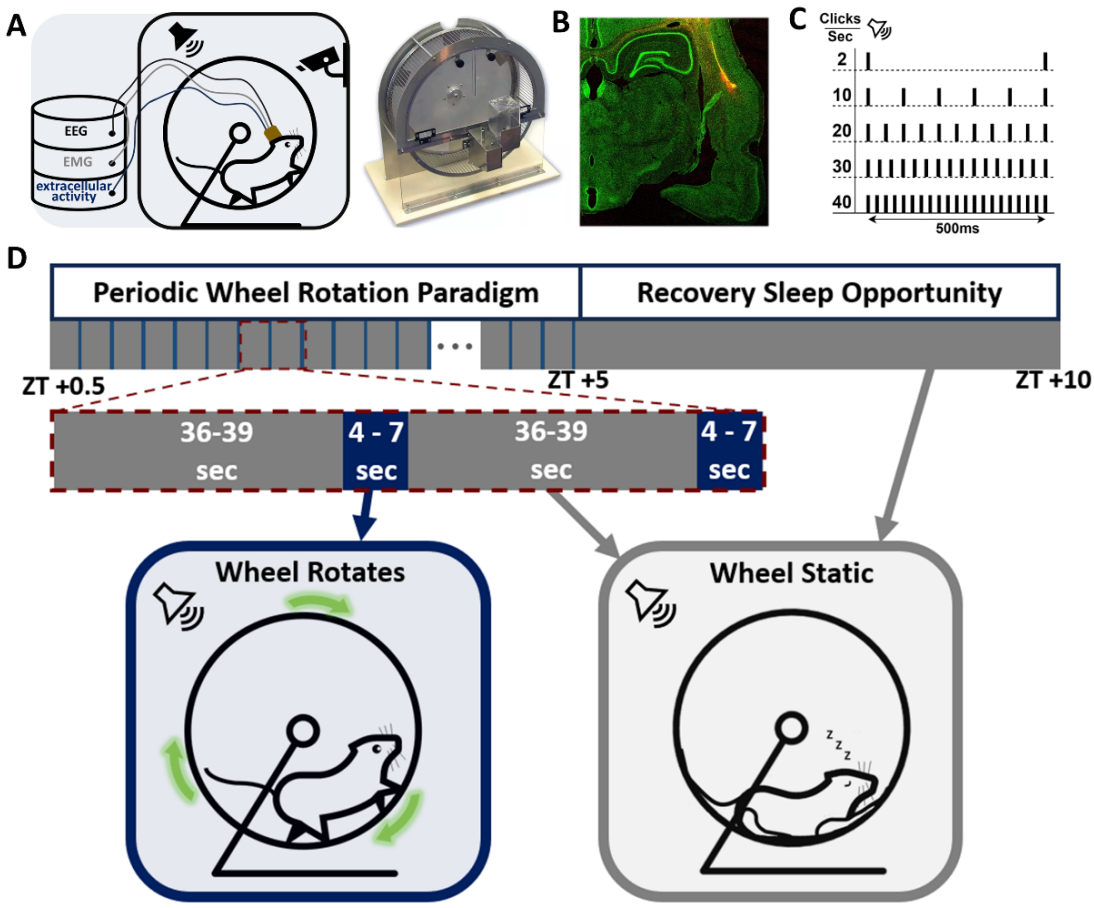

Figure 1. Experimental Setup. (A) (left): Acoustic chamber with an ultrasonic speaker and video monitoring, in which rats were confined to a motorized running wheel, while EEG, EMG, and

extracellular neural activity were measured continuously. (right): Motorized running wheel (Lafayette instrument), to which the rats were confined. (B) Histology of microwire traces targeting the auditory cortex. (C) Click-trains at varying rates presented throughout the experiment (D) Schematic depiction of the experimental paradigm. For the first 5h (zeitgeber time [ZT] 0–5), rats were intermittently forced to perform a short running bout with breaks allowing them to fall asleep. It was followed by 5h of undisturbed recovery sleep opportunity (zeitgeber time [ZT] 5–10). Auditory stimuli were presented throughout the entire experiment.

In the first 5h part of the experiment (periodic wheel rotation paradigm), rats often (44.3%) fell asleep during idle intervals and awakened with each wheel rotation, thereby presenting numerous isolated episodes of falling asleep (n=2,971 total, 186 ± 12.1 per session in n=16 sessions, mean ± SEM, Figure 2A, 2B, 2D). The second 5h part of the experiment (recovery sleep opportunity) also resulted in a substantial number of falling asleep episodes (n=2,996 total, 187± 16.6 per session, mean ± SEM, Figure 2A, 2C, 2D), as well as many spontaneous awakenings (n=2,718 total, 170± 17.2 per session, mean ± SEM, Figure 2A, 2B, 2D). In total, data analysis was performed for 5967 episodes of falling asleep and 2718 episodes of awakening.

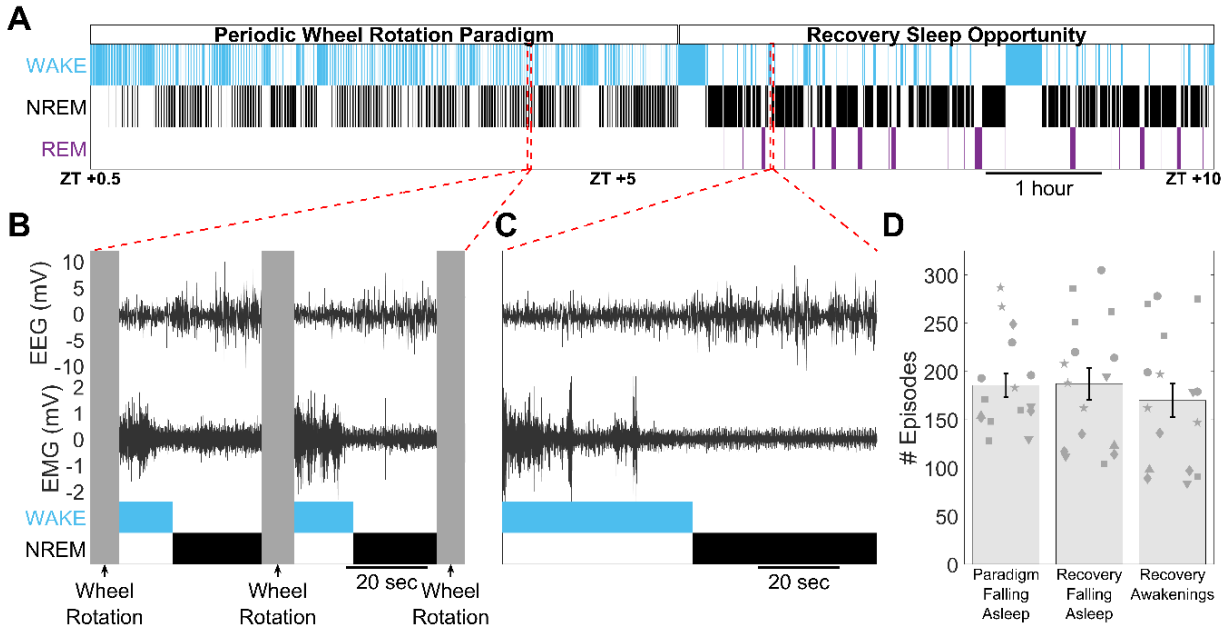

Figure 2. Capturing moments of falling asleep with polysomnography. (A) Representative hypnogram of a typical 10h session. Rows mark epochs of wakefulness (cyan), NREM sleep (black), and REM sleep (purple). Red dashed lines mark two example moments of a rat falling asleep – either between wheel rotations or during subsequent recovery sleep. (B) Representative Polysomnography of a trial of a rat falling asleep during two consecutive 40s intervals between brief (5s) wheel rotations (vertical gray bars). Rows (top to bottom) mark EMG, EEG, and automatically scored vigilance state (top – wake, cyan; bottom – NREM sleep, black) as in panel A. (C) Same as B, but for an example of a rat falling asleep during the recovery sleep opportunity period. (D) Count distribution across all sessions (n = 16) of falling-asleep instances during the periodic wheel rotation paradigm, as well as falling-asleep instances and awakenings during the recovery sleep opportunity period (left to right, respectively).

Identifying episodes of falling asleep and awakening

We first set out to automatically identify each falling asleep episode. To this end, we implemented the neural network-based automated AccuSleep algorithm (Barger et al., 2019) (Methods, Figure 3). The algorithm was trained on 1h-long manually-scored recovery period data containing intervals of wakefulness, non-rapid eye movement (NREM) sleep, and rapid eye movement (REM) sleep. We focused on the first hour of the recovery sleep opportunity that likely represents the deepest NREM sleep, in an effort to take a conservative approach in recognizing NREM and falling asleep episodes that refrains from subsequent analysis of borderline cases. Assessing the performance of the automatic sleep scoring method on the three sessions where sleep scoring was conducted fully (~10h each) we found that 93 ± 1.09 % of automatically scored 1s epochs correctly matched their corresponding manually scored labels (Figure 3D).

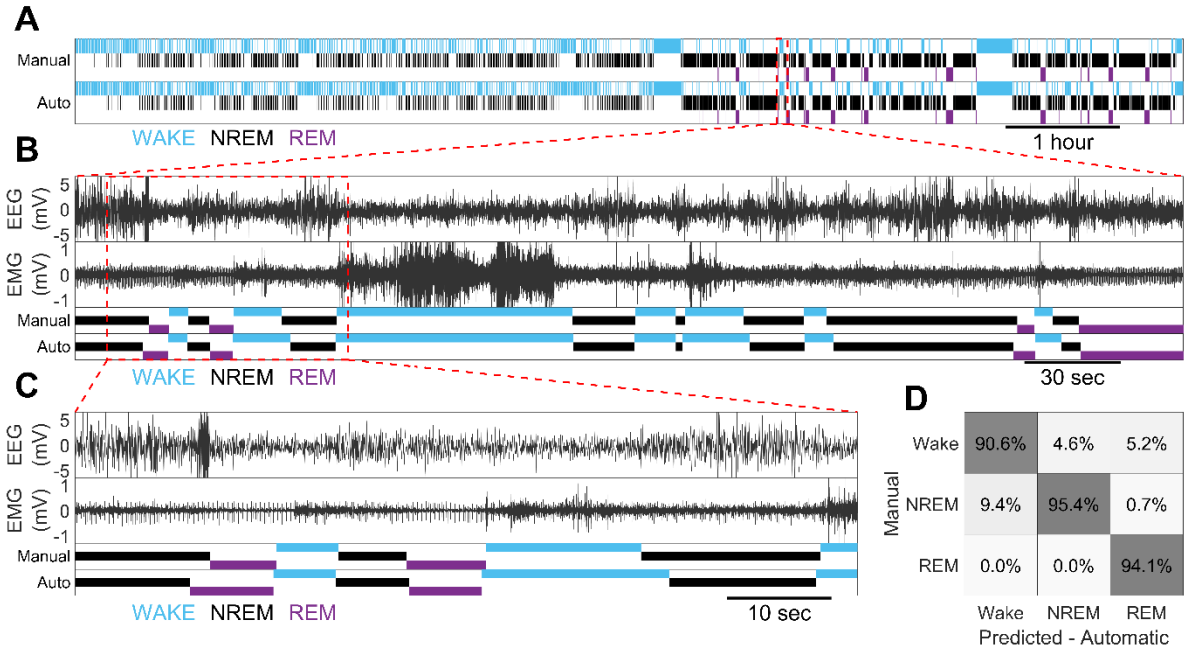

Figure 3. Automated sleep scoring by neural network for extracting falling asleep epochs. (A) Comparison of manual and automated sleep scoring of a representative session ~9h (top and bottom hypnograms, respectively). Red rectangle marks an example 6-minute segment of vigilance and sleep state changes expanded in panel B. (B) Polysomnography of a representative 6-minute segment. Rows (top to bottom) mark EMG, EEG, and manually and automatically scored vigilance state, as in A. Red rectangle marks further focus on 75 seconds expanded in panel C. (C) Same as in B, but for a shorter 75-second segment. (D) Confusion matrix between the vigilance states scored by automatic and manual sleep scoring over 3 sessions (~28h). Along the diagonal is the percentage of the automatically scored labels (column) that match the manually scored labels (row). Outside of the diagonal is the percentage of the automatically scored labels that do not match the manually scored labels but match the label of the relevant row.

Falling asleep suppresses sound-evoked post-onset neuronal firing within seconds

To analyze how neural processing and sensory responses in the auditory cortex changed around falling asleep with fine temporal resolution, we defined three intervals around wake-sleep transitions: "wakefulness" (-20 to -5sec before falling asleep), "First seconds of NREM" (+5 to +10sec after falling asleep), and "NREM" (>+60 after falling asleep). Based on our previous study on state-dependent auditory processing (Marmelshtein et al., 2023), we hypothesized that features of auditory cortical processing such as onset responses will maintain their magnitude when falling asleep, whereas features such as post-onset neuronal firing and population synchrony may be modulated during the process.

Figure 4A provides an example neuronal response of a representative unit to click stimuli, with trials vertically arranged according to their timing relative to the moment of falling asleep (top to bottom on y-axis). As can be seen for this unit (Figure 4A), as well as the average response (Figure 4B, n=152 units, 7 sessions), the onset response magnitude did not change around falling asleep (comparing wakefulness and first seconds of NREM). In contrast, the post-onset period (30-80 ms following sound onset) showed differences already during the first seconds of NREM sleep, in line with our hypothesis.

Expanding the analysis to all units (n=317) and multiple features of auditory processing (Figure 4C-E) revealed that onset response did not significantly change upon falling asleep, i.e. when comparing wakefulness and NREM sleep (Figure 4E, gray shading, -6.08% ± 4.65%, $p = 0.19$, $t_{316} = -1.31$, LME [Linear Mixed Effects Model]). Spontaneous firing rate and population synchrony exhibited moderate modulation (Figure 4C-E, gray shadings; -14.6% ± 5.81%, $p = 0.013$, $t_{316} = -2.51$ for reduction in spontaneous firing; 15.6% ± 4.26%, $p = 2.9 \times 10^{-4}$, $t_{316} = 3.67$ for elevation in population synchrony, LME). The most notable change was observed for post-onset neuronal firing (n = 152 units), which was strongly modulated between wakefulness and NREM, as can be seen in Figure 4A-D (gray shadings) and as evident quantitatively (-56% ± 4.3%, $p = 1.2 \times 10^{-26}$, $t_{151} = -13.1$, Figure 4E).

We further examined whether changes occur already within the first few seconds after falling asleep or, alternatively, reflect changes due to more consolidated NREM sleep within tens of seconds. As can be seen in the example unit in Figure 4A (dark blue) and the population response (Figure 4B, dark blue), post-onset firing was already significantly modulated within seconds after sleep onset. Quantifying this for the entire dataset (Figure 4C-E, n=317 units) revealed a sharp variation in post-onset firing within seconds of falling asleep (-51.2% ± 4.94%, $p = 2.5 \times 10^{-19}$, $t_{151} = -10.4$, comparing wakefulness to first seconds of NREM). Changes in spontaneous firing rate, although more moderate, also occurred within seconds (-17.8% ± 5.47%, $p = 1.2 \times 10^{-3}$, $t_{316} = -3.26$). In contrast, changes in

population synchrony were slower to occur and did not show significant modulation in the first seconds of NREM (2.26% ± 5.82%, $p = 0.69$, $t_{316} = 0.38$). Analysis of variance among the distinct features of

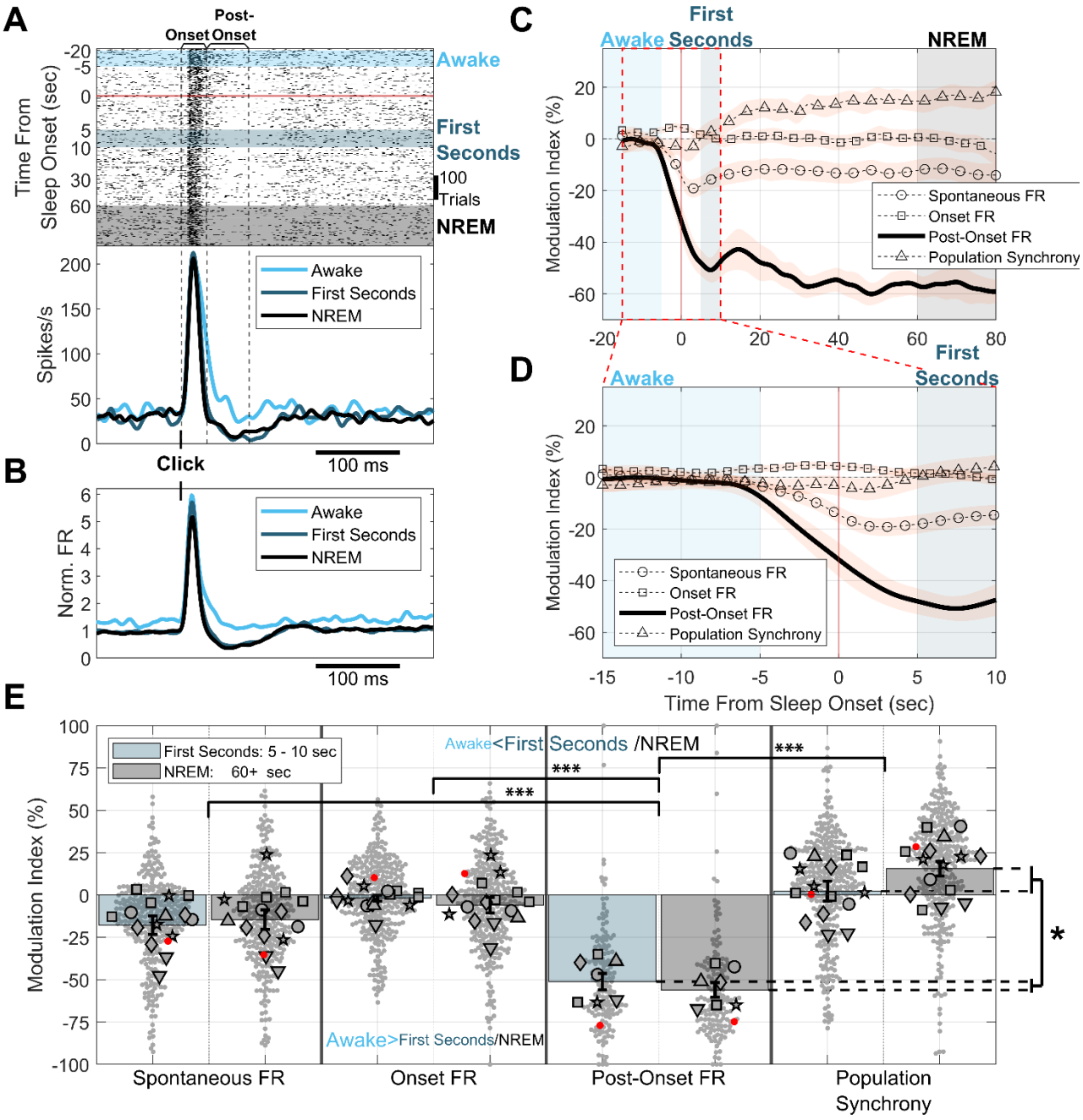

Figure 4. Post-onset firing changes within first seconds of falling asleep. (A) Representative raster and peristimulus time histogram (PSTH) for a unit in response to a click. Raster trials (rows) are ordered according to stimulus time relative to the proximate falling asleep instance. Azure, dark blue, and black shadings mark if the stimulus occurred while the animal was awake, in the first seconds after falling asleep, or during NREM sleep >60s after falling asleep, respectively. (B) Peristimulus time histogram of the mean normalized response to a click of all responsive units (n = 152, 7 sessions) during wakefulness, first seconds of NREM sleep, and NREM sleep following 60 seconds after the moment of falling asleep. (C) Modulation Index of activity and response features depending on stimulus time relative to the moment of falling asleep for all units (n = 152, 7 sessions for Post-Onset FR and n = 317, 15 sessions, for the other features). Azure, dark blue, and black shadings mark the "awake", "first

seconds of NREM", and "NREM" Periods as in A. Red rectangle marks the time range expanded in panel D. Yellow shading represents the standard error of the mean (SEM). (D) Same as C, but expanding the 25s around the moment of falling asleep. (E) Modulation Index of activity and response features between the states of "first seconds NREM" and "awake" (dark blue) and between the states "NREM" and "awake" (grey) across units and sessions (n = 152, 7 sessions for Post-Onset FR and n = 317, 15 sessions, for the other features). Bars and black error bars represent the mean ± SEM estimated by the Linear Mixed Effects model. Small grey markers represent individual units (red for the representative unit in panel A). Large grey markers represent individual session mean (with each shape representing an individual animal).

cortical auditory processing confirmed that they are differentially modulated within the first second of NREM ($p = 2.1\times10^{-4}$, n = 6 animals, Friedman test). In addition, upon entering a deeper state of NREM sleep, processing features were also differentially modulated ($p = 1.1\times10^{-4}$, n = 6 animals, Friedman test). Pairwise comparisons revealed that post-onset firing was modulated significantly more strongly than the other three features ($p < 2.1\times10^{-10}$, df = 151, for all three features within first seconds of NREM, and for all three features within NREM state, $p < 1.6\times10^{-14}$, df = 151, LME). The slower buildup of population synchrony can be appreciated most clearly when contrasting Figure 4C (robust changes in temporal dynamics at a scale of tens of seconds) with Figure 4D (no changes in temporal dynamics in first seconds). Indeed, a direct comparison established that the difference between the first seconds of NREM and deeper NREM was significantly larger for population synchrony modulation than for post-onset modulation (p = 0.023, df = 151, t151 = 2.3, LME).

Awakening restores sound-evoked post-onset neuronal firing within seconds

Does cortical auditory processing show an opposite profile upon awakening to that observed when falling asleep? To test this, we compared neuronal activity in the seconds just before awakening ("Sleep", -20 to -5sec before awakening) and just after awakening ("First seconds of wakefulness, +5 to +10sec after awakening). Figure 5A provides a representative example of a unit firing around awakening. As can be seen, post-onset activity rapidly changes from silence during sleep to firing in wakefulness, whereas population synchrony is minimally affected at these time-scales.

Quantifying these effects across the entire dataset (n=315 units, Figure 5A-D), we found a modest albeit significant increase in onset firing rate that occurred in the first seconds of wakefulness (11.7% ± 3.82%, $p = 2.6 \times 10^{-3}$, $t_{314} = 3.04$, LME). Similarly, we found moderately higher modulation indices representing elevation in spontaneous firing rate (19.8% ± 6.72%, $p = 3.5 \times 10^{-3}$, $t_{314} = 2.94$). As observed upon falling asleep, changes in post-onset firing were most pronounced and occurred within the first seconds of state transitions (n = 145 units, 42.3% ± 5.46%, $p = 1.6 \times 10^{-12}$, $t_{144} = 7.74$). Population synchrony, as was the case when falling asleep, did not significantly change within the first

few seconds around state transitions (-5.2% ± 4.2%, $p = 0.22$, $t_{314} = -1.23$). Together, awakening exhibits a "mirror-image" of the changes in cortical auditory activity to those found around falling asleep, with post-onset firing remaining the aspect that changes most strongly and rapidly. Analysis of variance among the distinct features of cortical auditory processing confirmed that they are differentially modulated within the first second of wakefulness ($p = 3.3\times10^{-4}$, n = 6 animals, Friedman test). Pairwise comparisons revealed that post-onset firing was modulated significantly more strongly than the other three features ($p < 3.8\times10^{-6}$, df = 144, for all three features, LME).

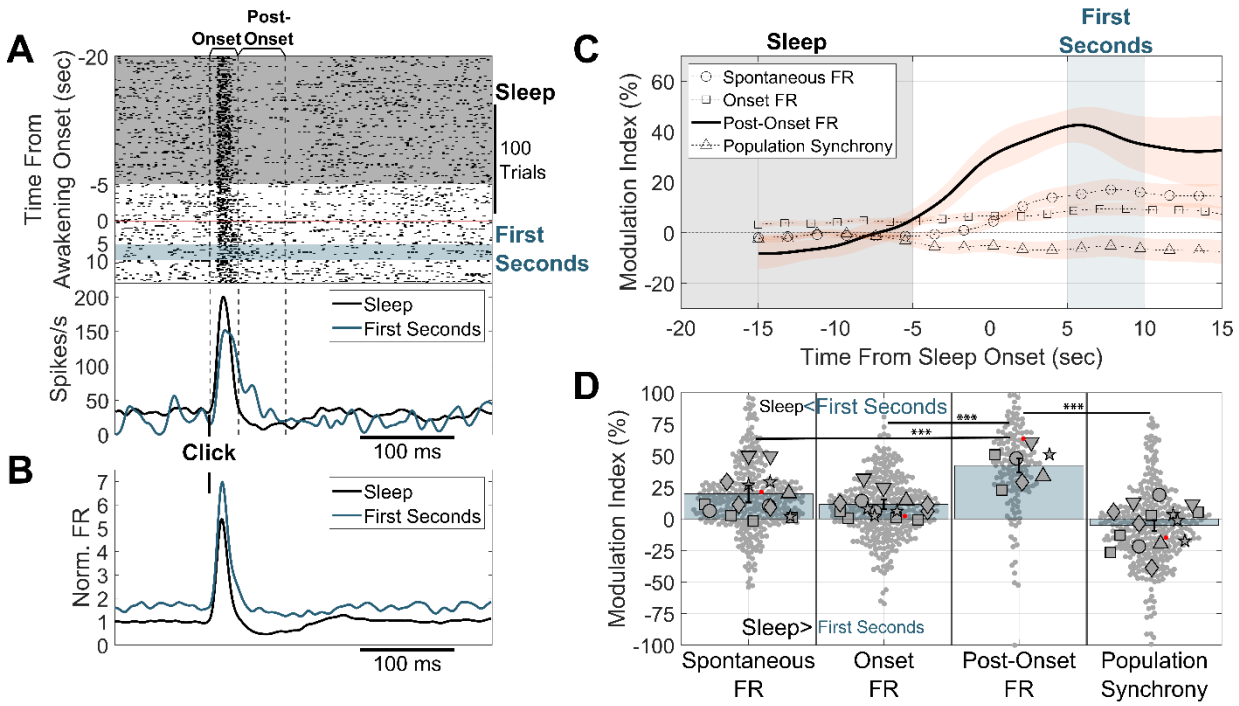

Figure 5 post-onset firing changes within first seconds of awakening. (A) Representative raster and peristimulus time histogram (PSTH) for a unit in response to a click. Raster trials (rows) are ordered according to the trial's stimulus time relative to the proximate awakening instance. Black and blue shadings mark if the stimulus occurred while the animal was asleep or in the first seconds after waking up, respectively. (B) Peristimulus time histogram of the mean normalized response to a click of all responsive units (n = 145, 7 sessions) during sleep and first seconds of wakefulness. (C) Modulation Index of activity and response features depending on stimulus time relative to the moment of awakening. Black and blue shadings mark "sleep" and "first seconds of wakefulness" periods as in A. Yellow shading represents the standard error of the mean (SEM). (D) Modulation Index of activity and response features between "first seconds wakefulness" and "sleep" states across units and sessions (n = 145, 7 sessions for Post-Onset FR and n = 315, 15 sessions, for the other features). Bars and black error bars represent the mean±SEM estimated by the Linear Mixed Effects model. Small grey markers represent individual units (red for the representative unit in panel A). Large grey markers represent individual session mean (with each shape representing an individual animal).

262 **Falling asleep modulates EEG auditory-evoked potentials within seconds**

263 Are changes in neuronal post-onset firing and population synchrony also captured by the EEG? We
264 sought to test this, seeking to relate our findings to the rich literature studying falling asleep with EEG.
265 To this end, we followed the same approach, comparing the EEG recorded from a screw over the frontal
266 lobe across three predefined intervals (Fig 6A-C) of "wakefulness" (-20 to -5sec before falling asleep),
267 "First seconds of NREM" (+5 to +10sec after falling asleep), and "NREM" (>+60 after falling asleep).
268 EEG auditory evoked potentials (AEPs) in response to click stimuli exhibited rapid changes within
269 seconds upon falling asleep (Fig 6A). As was the case in auditory cortex neuronal activity, an initial large
270 positive deflection in the AEP was unchanged before and after sleep onset. By contrast, a late large
271 negative deflection in the AEP occurring at the time of the neuronal post-onset firing period was
272 strongly modulated within the first seconds of NREM sleep (magnitude of 301±64% relative to
273 wakefulness, p=0.016, n=7 sessions, Wilcoxon Sign-Rank Test [WSRT]).

274 We quantified the temporal dynamics of this effect across all sessions by obtaining the AEP negative
275 deflection magnitude (methods) and calculated a running modulation index (Fig. 6B, C, trace with
276 asterisks) as for the previous auditory cortex neuronal response features (Fig. 4C,D). The AEP negative
277 deflection showed temporal dynamics qualitatively similar to the post-onset response in the auditory
278 cortex, both reaching their maximal change within seconds after falling asleep and then plateauing.
279 Qualitatively similar results, but with opposite direction, were observed upon awakenings (Fig. 7). We
280 also examined how EEG baseline (pre-stimulus) slow wave activity (SWA, power < 4Hz) depends on
281 falling asleep (Fig. 6B,C, diamonds), given its relation to synchronous neuronal activity (Vyazovskiy et
282 al., 2009). SWA increased within seconds upon falling asleep (Fig. 6C, 277±40% relative to wakefulness,
283 p=0.016, n=7 sessions, WSRT) but also continued to increase slowly afterwards (Fig. 6C, triangles,
284 437±56% relative to wakefulness), exhibiting a significant further increase from the "First seconds of
285 NREM" to subsequent "NREM" intervals (p = 0.031, n=7 sessions, WSRT).

286 Next, we examined the relation between neuronal activity measures (post-onset firing and population
287 synchrony) and EEG AEP measures (AEP negative deflection and SWA) at the single-trial level (Fig. 6D-
288 I). We selected a subset of trials with similar timing relative to the moment of falling asleep and divided
289 them into four quartiles according to their auditory cortex post-onset firing (methods). This created
290 four groups of trials with different average post-onset firing (Fig. 6D left) that were temporally balanced
291 across the falling asleep process (i.e. similar number of trials before, during, and after falling asleep in
292 each group). The four trial groups did not differ in their average auditory cortex population synchrony
293 (Fig. 6D right, p=0.543, n=7 sessions, Friedman test) implying that the two neuronal measures are
294 governed by fundamentally different processes. Strikingly, when extracting the EEG AEP for each of

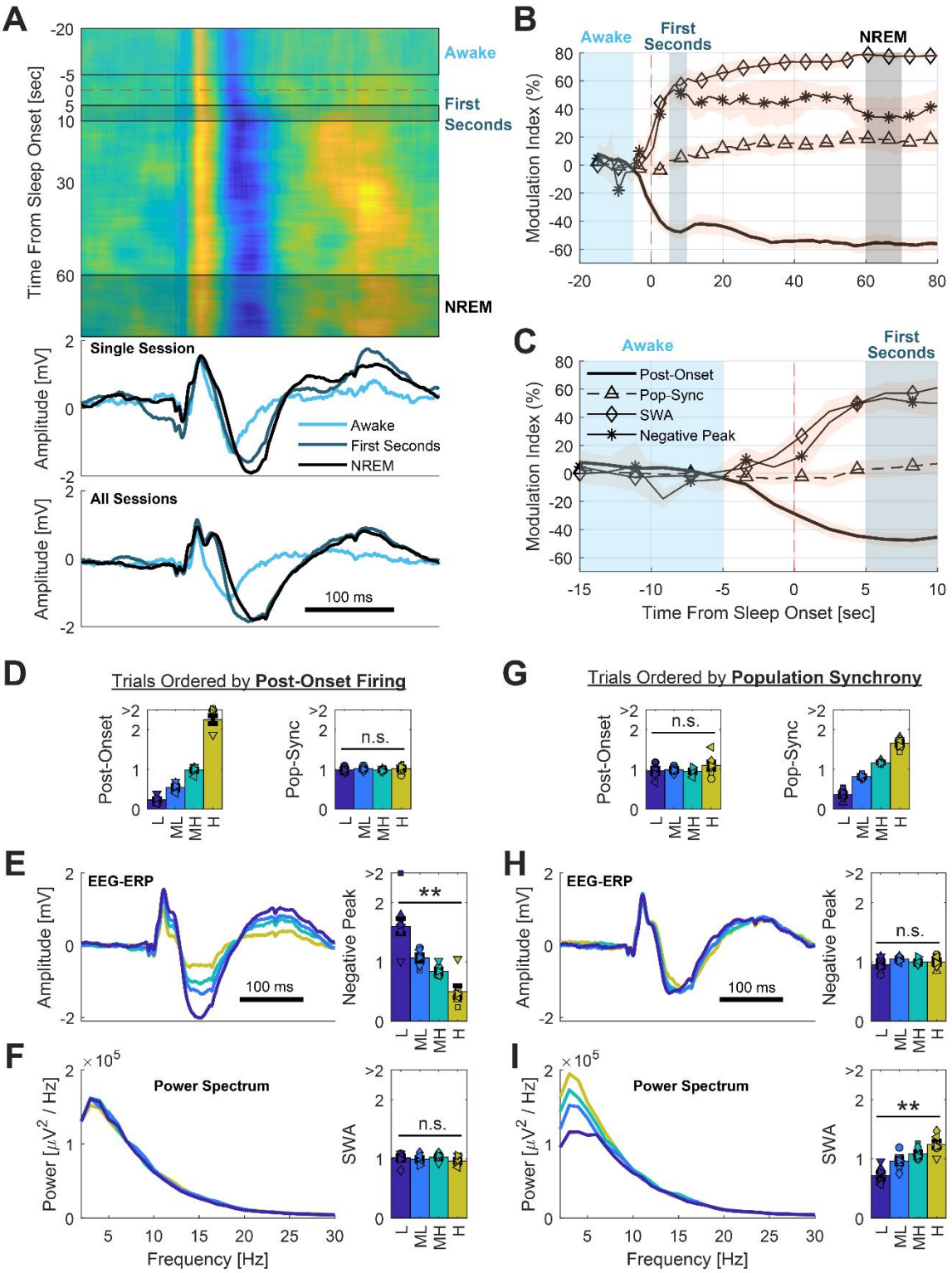

Figure 6. EEG AEP changes within first seconds of falling asleep. (A) Top: changes upon falling asleep in frontal EEG auditory evoked potential (AEP) following a click stimulus in a single representative session. Individual trials were sorted according to stimulus time relative to the proximate falling asleep instance. Each row represents an average AEP of 100 consecutive trials. Shadings mark if the stimulus occurred while the animal was awake, in the first seconds after falling asleep, or during NREM sleep >60s after falling asleep, respectively. Middle: Average AEPs for the three different intervals in a single

session. Bottom: Same as middle panel, but averaged across all sessions (N=7). (B) Temporal dynamics upon falling asleep of the modulation index of frontal EEG features, as well as auditory cortex neuronal features for comparison, averaged across all sessions (N=7). Frontal EEG AEP negative deflection and slow-wave activity (SWA) are marked by asterisk and diamond traces, respectively. Post-onset firing and population synchrony in auditory cortex neurons are marked by thick and triangle (dashed) traces, respectively. (C) same as B but with temporal axis expanded. (D-F) trials were sorted into four quartiles based on their relative auditory cortex post-onset firing (low post-onset FR (L), medium-low (ML), medium-high (MH) and high(H). (D) Auditory cortex normalized post-onset firing (left) and population synchrony (right) averaged across all sessions for the four different trial groups. (E) Average frontal EEG AEP (left) and its negative deflection magnitude (right) for the four different trials groups across all sessions. (F) Average baseline (pre-stimulus) power spectrum (left) and slow-wave activity (right, power for frequencies ≤4Hz) for the four different trials groups across all sessions. (G-I) same as D-F but with trials sorted into four quartiles based on their relative population synchrony in auditory cortex (low population synchrony (L), medium-low (ML), medium-high (MH) and high(H)).

these four groups, strong differences emerged (Fig. 6E left) with significant and reliable parametric modulation of the negative deflection magnitude (Fig. 6E right, p=0.0083, n=7 sessions, Friedman test). Importantly, no changes in baseline SWA were observed between the four different groups (Fig. 6F, p=0.419, n=7 sessions, Friedman test). Thus, post-onset firing in auditory cortex is specifically associated with the AEP negative deflection.

We then performed the same analysis, but now dividing trials based on their relative auditory cortex population synchrony (Fig. 6G-I). This process now created four groups that were different in their population synchrony (Fig. 6G right), but that showed no difference in their average post-onset firing (Fig. 6G left, p=0.319, n=7 sessions, Friedman test). This led to an exactly opposite pattern, without observable EEG AEP differences between the groups (Fig. 6H, p=0.419, n=7 sessions, Friedman test) but with significant and reliable parametric differences in SWA (Fig. 6I, p=0.002, n=7 sessions, Friedman test). Qualitatively similar results were also observed upon awakenings (Fig. 7). Overall, this analysis establishes that reduced post-onset firing in auditory cortex neurons is selectively associated with the EEG AEP late negative deflection, while auditory cortex neuronal population synchrony is selectively associated with EEG slow wave activity, thereby revealing a robust double-dissociation between the two auditory cortex measures and the two EEG phenomena.

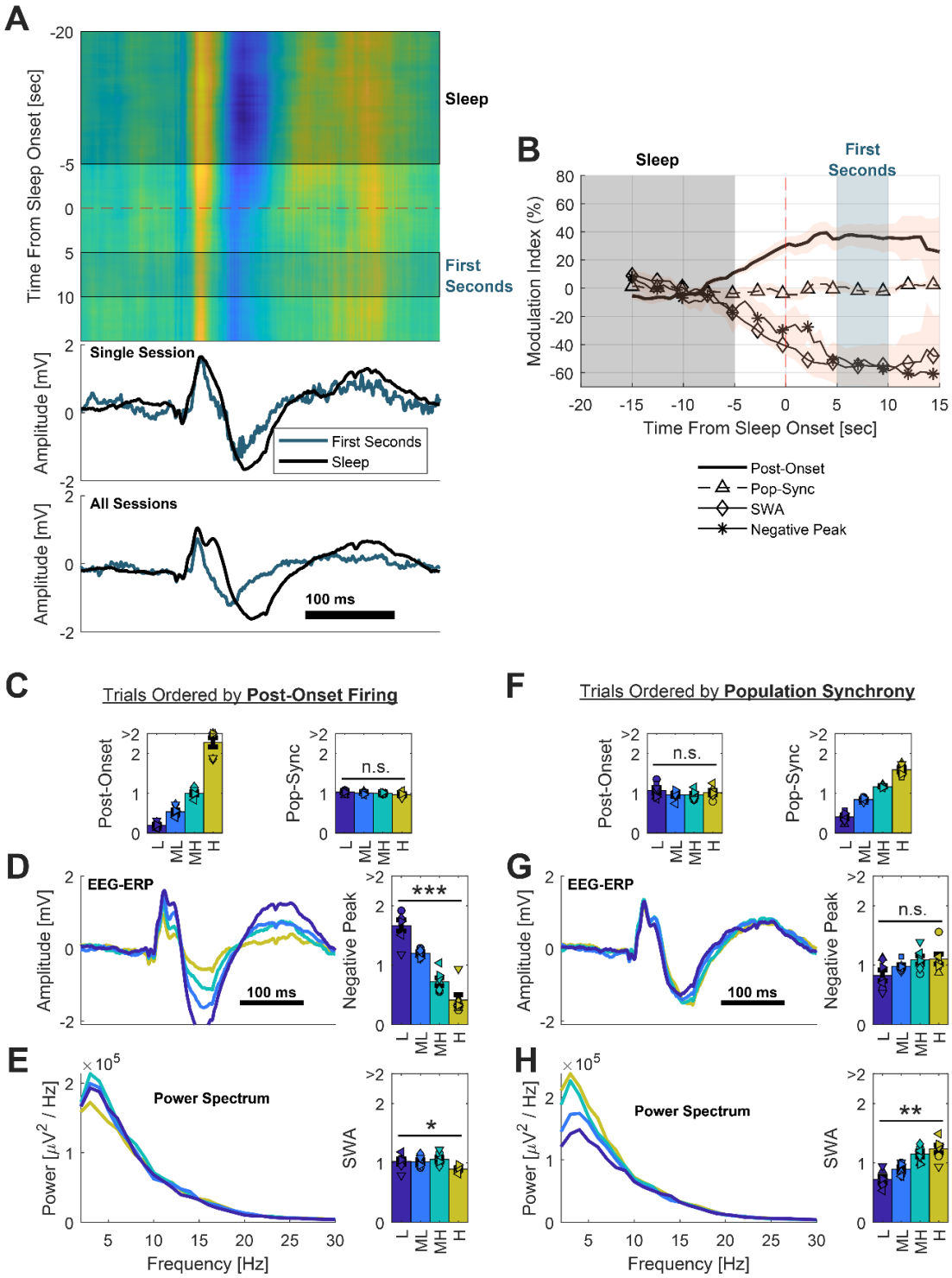

Figure 7. EEG AEP changes within first seconds of awakening. Same as figure 6 but for awakenings. (A) Top: changes upon awakenings in frontal EEG auditory evoked potential (AEP) following a click in a single representative session. Individual trials were sorted according to stimulus time relative to the proximate awakening instance. Each row represents an average AEP of 100 consecutive trials. Shadings mark if the stimulus occurred while the animal was asleep, or during the first seconds after waking up. Middle: Average AEPs for the two different intervals in a single session. Bottom: Same as middle panel, but averaged across all sessions (N=7). (B) Temporal dynamics upon waking up of the modulation index of frontal EEG features, as well as auditory cortex neuronal features for comparison, averaged across

all sessions (N=7). Frontal EEG AEP negative deflection and slow-wave activity (SWA) are marked by asterisk and diamond traces, respectively. Post-onset firing and population synchrony in auditory cortex neurons are marked by thick and triangle (dashed) traces, respectively. (D-F) trials were sorted into four quartiles based on their relative auditory cortex post-onset firing (low post-onset FR (L), medium-low (ML), medium-high (MH) and high(H). (D) Auditory cortex normalized post-onset firing (left) and population synchrony (right) averaged across all sessions for the four different trial groups. (E) Average frontal EEG AEP (left) and its negative deflection magnitude (right) for the four different trials groups across all sessions. (F) Average baseline (pre-stimulus) power spectrum (left) and slow-wave activity (right, power for frequencies ≤4Hz) for the four different trials groups across all sessions. (G-I) same as D-F but with trials sorted into four quartiles based on their relative population synchrony in auditory cortex (low population synchrony (L), medium-low (ML), medium-high (MH) and high(H)).

Discussion

We studied how neuronal spiking activity and responses to clicks in early rat auditory cortex change in the seconds around falling asleep and waking up. We found that increased post-onset neuronal silent periods (OFF states) and moderate reductions in spontaneous firing rates - both known to occur in NREM sleep (Marmelshtein et al., 2023) - changed abruptly around the first seconds of falling asleep. These changes in activity and responsivity during the first (~5sec) moments of sleep reached their full magnitude as observed in later consolidated NREM sleep (>60 sec from the moment of falling asleep). By contrast, an increase in neuronal population synchrony only changed substantially during later (>60 sec) NREM sleep without robust modulations around the seconds of falling asleep. Onset response magnitude was unaffected by falling asleep or awakening, echoing previous studies showing its invariance during sleep (Issa and Wang, 2008; Nir et al., 2013). During the first seconds after awakenings, we found opposite changes in neuronal activity and responsivity (rapid and robust decrease in the occurrence of post-onset silent periods, and rapid moderate elevation in spontaneous firing rates). These changes showed identical temporal dynamics, but with opposite directionality, to those observed when falling asleep. Fast changes in EEG activities including modulations in baseline SWA and the AEP were also observed upon falling asleep and awakening. SWA was selectively associated with changes in auditory cortex population synchrony, whereas the AEP negative deflection was selectively associated with post-onset neuronal silence. Together, the results indicate that some changes in auditory cortex activity occur within seconds around wake-sleep transitions whereas specific aspects such as population synchrony vary with slower dynamics. Auditory-induced silent OFF periods emerge as the aspect that changes most robustly around state-transitions, showing abrupt and large changes in its magnitude within seconds. The tight correlation between auditory cortex activity and the EEG recorded over the frontal lobe imply that these changes are not limited to the auditory cortex.

How do the present results relate to previous studies on changes in auditory responses across states of arousal? A recent study examined the effect of gradual propofol anesthesia on auditory processing (Bergman et al., 2022). There, observed changes were gradual and tightly locked to increasing anesthetic concentration rather than to more abrupt loss of behavioral responsiveness. Furthermore, we recently showed that the degree of post-onset neuronal firing decreased gradually with mounting sleep pressure across several hours of sleep deprivation (Marmelshtein et al., 2023). Thus, gradual changes in arousal often lead to gradual changes in auditory processing. Here, however, we were able to examine, for the first time, abrupt transitions in arousal states around falling asleep and waking up

387 episodes. Under these conditions, we find that sharp step-like changes can occur at a timescale of few
388 seconds, as demonstrated for the decreased post-onset firing around sleep onset. Thus, we suggest
389 that arousal-related changes in neural responses can be either gradual or abrupt, depending on the
390 nature of the change in arousal state. Accordingly, gradual changes in arousal state (e.g. mounting
391 sleep pressure or deepening anesthesia), will be associated with gradual changes in neural responses,
392 whereas abrupt changes in arousal state (e.g. falling asleep or awakening) will be associated with sharp
393 changes in neural responses.

394 Beyond neuronal correlates in specific pathways such as the auditory cortex, what do our findings
395 reveal more generally about falling asleep – is it fundamentally a gradual or abrupt process? While
396 extensive evidence shows that many electrical, physiological and behavioral phenomena change
397 gradually in the span of minutes (Ogilvie, 2001; Eban-Rothschild et al., 2016; Lacaux et al., 2023), some
398 EEG phenomena and specific measures of behavioral responsiveness do show fast temporal dynamics
399 (Ogilvie, 2001; Strauss et al., 2022). We find evidence supporting both of these seemingly contradicting
400 themes. On the one hand, post-onset neuronal silence changes rapidly within just few seconds upon
401 sleep onset. Exposing these fast dynamics relied critically on our ability to sleep score our data at high
402 temporal resolution (1 second). On the other hand, population synchrony displayed different temporal
403 dynamics, developing gradually on the time scale of one minute. Similarly, measures of EEG
404 information and connectivity also change on such a slow time-scale (Strauss et al., 2022). This implies
405 that these two measures may reflect different underlying neural processes both accompanying sleep
406 onset, one that is continuous and gradual, and another abrupt.

407 Examining the effects of falling asleep (and awakening) on EEG activity helps connect the observations
408 at the neuronal level to the non-invasive literature. The change in baseline (pre-stimulus) EEG SWA
409 upon falling asleep is not necessarily surprising, as these changes comprise the criteria used to define
410 wake-sleep transitions. By contrast, the fast change in the K complex-like AEP negative deflection
411 reached maximal modulation within seconds of falling asleep or awakening, thereby providing
412 independent evidence for rapid changes in brain activity upon sleep state transitions. Investigating
413 trial-by-trial variability allowed to establish direct link between EEG and neuronal-level phenomena,
414 revealing a double-dissociation between the EEG AEP and post-onset neuronal silence (changing
415 rapidly and reaching maximum change within seconds) versus population synchrony and ongoing EEG
416 SWA (continuing to change over longer time scales after state transitions).

417 The functional significance of increase in post-onset neuronal silence remains unclear. Considering the
418 strong association with the EEG AEP, It is highly likely that neuronal silence as captured in extracellular
419 recordings reflects a state of neuronal bistability where neurons alternative between active (up) and

hyperpolarized silent (down) states , a key feature of sleep and unresponsive states (Massimini et al., 2007; Vyazovskiy et al., 2011, 2013; Marmelshtein et al., 2023). While such bistability does not interfere with short-lived localized onset responses, it can disrupt complex neural processing by breaking-off sustained and widespread propagation of sensory signals (Massimini et al., 2005; Pigorini et al., 2015). Indeed, states of drowsiness and sleep associated with increased bistability affect processing requiring integration beyond local activity patterns. Accordingly, drowsiness preferentially disrupts perceptual discrimination, rather than perceptual detection (Xu et al., 2023). Moreover, measures of complex neural processing, such as predictive coding, are preferentially affected by sleep onset (Strauss et al., 2015), and baseline complexity measures were maximally attenuated in NREM sleep when stimuli evoked a k-complex, reflecting high neuronal bistability (Andrillon et al., 2016).

Certain limitations in our study require explicit acknowledgment. First, it is not trivial to generalize results about the precise dynamics around state transitions from rodents to humans and other species. Since rodents exhibit more fragmented sleep and shorter bouts of sleep and wakefulness (Lo et al., 2004), the first few seconds of sleep or wakefulness in rats may or may not be directly comparable to the first few seconds of longer sleep bouts. Nevertheless, the fact that some aspects of auditory processing changed robustly and abruptly (post-onset firing) whereas other aspects changed more modestly (ongoing firing rates) or more gradually (population synchrony) goes beyond differences across species. Second, while our recordings focused on (early) auditory cortex and AEPs in the EEG, the spatial scale of these effects remains unclear. Further studies are needed to examine to what extent such findings can be generalized to other sensory modalities and cortical areas. However, the selective relationship between auditory cortex post-onset responses and the frontal EEG AEP negative deflection suggests that such effects may be widespread. Finally, some limitations relate to our extracellular recordings, discussed also previously (Marmelshtein et al., 2023); these include a bias for larger pyramidal cells with high baseline firing rates as well as lack of information on cortical layer and cell types, possibly biasing our results towards specific neuronal subpopulations.

In conclusion, our investigation reveals the temporal dynamics and magnitude of modulation in different features of auditory processing upon falling asleep and awakening. Our findings extend previous studies in showing that specific neural signatures of auditory responses, particularly the degree of post-onset firing, are robustly influenced by vigilance states and their transitions (Marmelshtein et al., 2023). A rapid and robust dramatic increase in post-onset neuronal silence, occurring within seconds of falling asleep, contrasts with the slower modulation observed in population synchrony, and emerges as a robust signature of altered responsivity of the sleeping brain to external sensory stimuli.

454 # Methods

455 **Animals**

456 The study involved electrophysiology experiments in six adult male Wistar rats (weight: 300-350g, age:
457 >12 weeks). Rats were kept in transparent Perspex cages with food and water available ad libitum. The
458 ambient temperature was maintained between 20-24 Celsius, and there was a 12:12 hours light/dark
459 cycle with light onset at 10:00 AM. All experimental procedures, including animal handling, wheel cycle
460 paradigm, and surgery, were conducted in accordance with the National Institutes of Health's Guide
461 for the care and use of laboratory animals and approved by the Institutional Animal Care and Use
462 Committee of Tel Aviv University.

463 **Surgery and electrode implantation**

464 Before surgery, DiI fluorescent dye (DiIC18, Invitrogen) was applied to microwire arrays under
465 microscopic control to aid in localization. Generally, surgical procedures followed our previous
466 protocols (Sela et al., 2020b). First, isoflurane (4%) was used to induce general anesthesia, and animals
467 were then placed in a stereotactic frame (David Kopf Instruments). During the rest of the surgery,
468 anesthesia (isoflurane, 1.5-2%) and a 37C body temperature (closed-loop heating pad system, Harvard
469 Apparatus) were maintained. Animals were given antibiotics (Cefazolin, 20 mg/kg i.m.), analgesia
470 (Carpofen, 5 mg/kg i.p.), and dexamethasone (0.5 mg/kg, i.p.). Their scalp was shaved, and liquid gel
471 (Viscotears) was applied to protect their eyes. Subcutaneous infusion of lignocaine (7 mg/kg) was
472 performed before incision, and then the skull was exposed and cleaned. Two frontal screws (one on
473 each hemisphere, 1mm in diameter) and a single parietal screw (left hemisphere) were placed in the
474 skull for recording EEG. Two screws were placed above the cerebellum, serving as reference and
475 ground. Two single-stranded stainless-steel wires were inserted to the neck muscles to record EMG.
476 EEG and EMG wires were to a head-stage connector (Omnetics). Dental cement was applied to cover
477 all screws and wires. A small craniotomy was performed over the right hemisphere, and the dura was
478 meticulously dissected. An auditory cortex-targeting 16-electrode microwire array (Tucker-Davis
479 Technologies, TDT, 33 or 50mm wire diameter, 6-6.5 mm long, 15 tip angle; arrays consisting of 2 rows
480 3 8 wires, with 375mm medial-lateral separation between rows and 250mm anterior–posterior
481 separation within each row) was implanted diagonally (angle of 28 degrees, see Figure 1B) with
482 insertion point center coordinates of P: -4.30mm, L: 4.5mm relative to Bregma, and inserted until a
483 final depth of 4.6mm was reached. Silicone gel (Kwik-Sil; World Precision Instruments) was applied to
484 cover the craniotomy, and Fusio (Pentron) was used to fix the microwire array in place. After surgery,
485 chloramphenicol 3% ointment was applied topically, and buprenorphine (0.025 mg/kg s.c.) was given

systemically for additional post-operative analgesia. Dexamethasone (1.3 mg/kg) was given with food in the days following the surgery to reduce pain and inflammation around implantation.

Histology

After conducting the experiments, we confirmed the position of electrodes in 4 out of 6 animals through histology, as shown in Figure1B. Animals were anesthetized with 5% isoflurane and perfused with 4% paraformaldehyde. The brains were refrigerated in paraformaldehyde for a week and then cut into 50-60mm serial coronal sections using a vibrating microtome (Leica Biosystems). The sections were stained with fluorescent cresyl violet/Nissl (Rhenium). The histological verification ensured that the electrodes were located within areas Au1/AAF/AuD as defined by Paxinos and Watson (Paxinos and Watson, 2006).

Electrophysiology

Data were acquired using a RZ2 processor (TDT). Microwire extracellular activity was digitally sampled at 24.4 kHz (PZ2 amplifier), while EEG and EMG were pre-amplified (RA16LI , TDT) and sampled at 256.9 Hz (PZ2 amplifier, TDT). Spike sorting was performed with “wave_clus” (Quiroga et al., 2004), which utilized a detection threshold of five SDs and automatic superparamagnetic clustering of wavelet coefficients. The clusters were then manually selected, refined, and tagged as either multi-units (MU) or single-units (SU) based on their stability throughout the recording, quality of separation from other clusters, consistency of spike waveforms, and inter-spike interval distributions (N_{MU} = 332, N_{SU} = 88), as described in (Nir et al., 2015). We verified the accurate localization of the auditory cortex, which includes A1, the anterior auditory field, or the dorsal auditory cortex, using histology (Figure 1B) and by analyzing the units’ response latency to auditory stimuli (Marmelshtein et al., 2023).

Experimental Design

Following surgery, the subjects were housed separately and introduced to the motorized running wheel for a few hours every day for habituation (Figure 1A). They were then gradually introduced to the periodic wheel rotations to be performed in the first experimental phase (Figure 1D, see below). We conducted 16 experimental sessions in the following manner. At the start of the day (10 AM), the rats were moved from their home cage to a motorized running wheel (Figure 1A, Model 80860B, Lafayette Instrument) placed within a sound-attenuation chamber (-55dB, H.N.A) and underwent five hours of periodic wheel rotation. During the first experimental phase, the wheel was rotated for 3 seconds every 36-39 seconds, which constituted intervals when rats could behave freely (run, groom, or fall asleep). In the second experimental phase, rats were allowed to rest undisturbed for an additional 5 hours in the (fixed) wheel, which constituted a recovery sleep opportunity (Figure 1D).

The rats were kept in the wheel apparatus under the ultrasonic speaker for the entire session. Auditory stimulation was delivered intermittently throughout both the sleep deprivation and recovery sleep periods, irrespective of the wheel's movement.

Auditory stimulation

We used Matlab (MathWorks) to compile sound waveforms that were then transduced into voltage signals using a high-sampling rate sound card (192 kHz, LynxTWO, Lynx). These signals were amplified (SA1, TDT) and played through a magnetic speaker (MF1, TDT), mounted 60 cm above the motorized running wheel. We conducted two different auditory experiments over separate sessions/days:

Auditory paradigm A

This paradigm was used in 7 sessions in 6 animals: Stimuli included click trains and a set of Dynamic Random Chords (DRC)(Linden et al., 2003). Click trains lasted 500ms and were played at rates of either {2, 10, 20, 30, 40} clicks/sec (Figure 1C). A typical 10-hour session contained 2000 blocks, each consisting of a single DRC stimulus and a single repetition of each click train (presented at random order), with an inter-stimulus interval of 2s and ±0.25s jitter.

Auditory paradigm B

This paradigm was used in 9 sessions in 5 animals: The stimuli used in the study included a 40 clicks/second click-train and a set of DRC stimuli. Each 10-hour session had 600 blocks, with each block consisting of a single DRC stimulus and 4 repetitions of the 40 Hz click train, presented in random order. The inter-stimulus interval was 2 seconds, with a ±0.25-second jitter. Both paradigms included an 8-second inter-stimulus interval every 2 minutes.

Acoustic sound-level measurements

We used a high-quality ultrasonic microphone (model 378C01, PCB Piezotronics) to measure sound levels at 12 positions around the circumference of the wheel apparatus (anterior-posterior axis) and at five positions along its width (left-right axis) with a spacing of 2cm. This covered the area where animals were present during the experimental sessions. We found that the root-mean-square (RMS) intensity in response to 2-second white noise sounds had minimal variance at different positions along the anterior-posterior axis, with a mean absolute deviation of 0.7±0.3dB (±Std. Dev) and a maximum difference of 2.4dB between any two positions. Similarly, along the left-right axis, we recorded a mean absolute difference of 0.4±0.3dB (±Std. Dev.) and a maximum difference of 1.5dB. When we examined sound levels at different frequency bands (1, 2, 4, 8, 16, 32, and 64 KHz, in response to the same white noise stimulus) at different positions, we found similarly low variation (all below 4dB)).

Sleep scoring and identification of state transitions

In each session (n=16), at least one hour (the last hour, representing recovery sleep opportunity period) was manually sleep scored, employing visual inspection of EEGs, EMGs, and video/behavior as in previous studies (Vyazovskiy et al., 2011; Rodriguez et al., 2016; Sela et al., 2020a). In an additional three sessions, manual sleep scoring of the entire 8-9h experiment was performed and used for assessing the performance of automatic sleep scoring (Figure 3A-D).

Before any sleep scoring, we excluded any periods when the wheel was moving (forced running bouts during the first experimental phase). Next, we categorized different time periods to either active-wakefulness with behavioral activity (e.g., locomotion, grooming) as confirmed by video, quiescent-wakefulness (low-voltage high-frequency EEG activity and high tonic EMG with occasional phasic activity), NREM sleep (high-amplitude slow wave activity and low tonic EMG activity), REM sleep (low-amplitude wake-like frontal EEG co-occurring with theta activity in parietal EEG and flat EMG, Figure 2A-C), or unknown periods not analyzed further (e.g. state transitions, to conservatively avoid these epochs in subsequent analysis).

Next, the 1h+ manually-scored data in each session was used to train an automated sleep-scoring algorithm using convolutional neural networks (CNNs) (Barger et al., 2019). The algorithm was fed with the manual sleep scoring vector along with the frontal EEG signal (low-pass filtered < 60Hz), and the EMG signal (band-pass filtered 10Hz – 125Hz). Manually scored labels, originally tagged in 1ms resolution, were re-labeled into 1sec epochs, where each epoch was labeled according to the most frequent manual label in that interval. For each rat, a personalized CNN was trained using the manually labeled data of all the sessions of the same rat (1-4 sessions per rat). Weights for mixture z-scoring, for both training and classification, were calculated using the relative prevalence of each state in the data used for training. Epoch length was 1 sec. The CNNs trained with consideration of 9 epochs surrounding each epoch scored (four epochs preceding and four epochs following the current epoch). Calibration data for mixture z-scoring for classification was also provided as the training data. Using the relevant rat's CNN for each session, the entire data set was classified into the sleep scoring labels. After applying the classification method, we designed a post-processing method for the labels to meet our goal for early detection of true fall-asleep (awakening) transitions. In which case, for each session, the epochs labels were examined from the last one to the first one. Epochs with low certainty levels in all states, i.e., below 50%, were set to be the same as the label of the following epoch (the later in time). Then, epochs that were labeled differently from their two neighboring (preceding and following) epochs, and their neighbors had the same label, were changed to match their neighbors. Any epochs containing times when the wheel was moving were excluded from the analysis.

582 Extracting falling asleep and awakening episodes, based on the automatic sleep scoring, was
583 performed as follows. We considered a falling asleep instance as a continuous sequence (≥2 sec) of
584 NREM epochs (epoch = 1 sec), preceded by a continuous sequence (≥2 sec) of quiescent-wakefulness
585 epochs. The beginning of the first NREM epoch was considered, for our matter, the moment of falling
586 asleep. For the subsequent analysis of neural activity, a symmetrical time window around the falling
587 asleep moment was taken. The window extended as long as possible without including periods of rat
588 movement, wheel movement, or epochs that are not part of quiescent-wakefulness or NREM
589 sequences. Falling asleep instances were discarded from the subsequent analysis if more than one
590 falling asleep transition occurred within the same 36-39sec interval between consecutive wheel cycles.
591 Awakening instances were extracted only from the spontaneous sleep opportunity phase. We
592 considered an awakening instance in a similar way, a continuous sequence of quiescent-wakefulness
593 epochs (≥2 sec), preceded by a continuous sequence (≥2 sec) of NREM epochs. The beginning of the
594 first quiescent-wakefulness epoch was considered, for our matter, the moment of awakening. For the
595 subsequent analysis of neural activity, a symmetrical time window around the awakening moment was
596 taken. The window extended as long as possible without including periods of rat movement, or epochs
597 that are not part of quiescent-wakefulness or NREM sequences. Falling asleep and awakening
598 instances with a time window shorter than 3 sec were not analyzed.

599

600 **QUANTIFICATION AND STATISTICAL ANALYSIS**

601 **Analysis of auditory responses across states**

602 Auditory stimuli presented during the times of wheel movement or while the rat was active
603 (locomotion, grooming for example) were excluded from analysis.

604 **Analysis of responses to click trains (Figures 4C, 4D, 4E, 5C, 5D, 6B, 6C)**

605 To measure spontaneous firing rate, we calculated the average firing rate during the [-500,0]ms
606 window leading up to the click-train stimuli. For post-onset firing rate, we calculated the average firing
607 rate during the [30,80]ms window. We analyzed onset response to different click rates using smoothed
608 peri-stimulus time histograms (PSTH) with a Gaussian kernel (σ=2ms). The onset response was
609 determined by extracting the highest firing rate during the [0,50]ms window of the smoothed PSTH.
610 Population synchrony was defined as population coupling (Okun et al., 2015) and calculated as the
611 correlation of each unit firing to that of the entire neuronal population average in 50ms bins during
612 the baseline period ([-1000,0]ms). We calculated population coupling for each trial baseline period
613 and then averaged for all trials in a given condition.

Feature modulation between states (Figures 4E, 5D)

For each session, all auditory stimulation trials that appeared around falling asleep (or awakening) episodes were sorted according to their time relative to the moment of falling asleep (or awakening). We defined three vigilance states in the falling asleep process: “wakefulness” / “First seconds of NREM” / “NREM”, with different time ranges relative to the moment of falling asleep (-20s < t < -5s, 5s < t < 10s, 60s < t; respectively). Two states were also defined for awakening episodes: “Sleep” / “First seconds of wakefulness” (-20s < t < -5s, 5s < t < 10s; respectively). Auditory trials around moments of falling asleep / awakenings were sorted into these states.

For each feature of auditory processing (spontaneous firing, onset response, population synchrony, post-onset firing), we pooled trials from all relevant click-trains presented (2,10,20,30,40 Hz): for spontaneous firing rate and population synchrony we examined baseline activity of all click trains; for onset firing rate, responses to all click trains; and for post-onset firing rate click trains of 2 Clicks/sec and 10 Clicks/sec (allowing sufficient inter click interval to not interfere with the post-onset period). Within the states and relevant stimuli pooled for each features the unit response among all trials was averaged resulting PSTH. The response analysis, as described for each feature was performed on each PSTH, gaining features value for all states. To compare responses between the vigilance states, modulation index was calculated between the feature’s value in the first seconds of NREM state (first seconds of wakefulness, for awakening) to the value in the wakefulness state (Sleep, for awakening) and between the feature’s value in the NREM state (wakefulness, for awakening) to the value in wakefulness state (Sleep, for awakening).

Modulation index between two conditions for all measures above was calculated as:

$$\frac{ConditionA - ConditionB}{max(ConditionA, ConditionB)} \times 100$$

Feature analysis along arousal state transitions (Figures 4A, 4C, 4D, 5A, 5C, 6B, 6C)

For each session and per each feature, auditory trials within falling asleep (awakening) episodes were extracted and sorted by time relative to the moment of falling asleep (awakening) as before, yielding a sorted unit response raster (Figure 4A). For each unit, the responses for adjacent trials (in terms of time relative to the moment of falling asleep/awakening) were smoothed (except for population synchrony) by a moving average window (uniformly weighted), with the size of 50 or 100 trials and an overlap of 49 or 99 trials (figures 4-5 and figure 6, respectively). Due to unevenly spaced stimuli’s relative times, new time stamps were created by smoothing the original stimuli relative times with the same method. Resulting in a modified raster where each row represents a 50-trial averaged response

and its average stimuli time. Thereafter, a modulation index was calculated between the averaged value of the feature in each (averaged) time stamp compared to that during “wakefulness” (“Sleep” for awakening) state. For population synchrony, the feature values were first calculated for each trial, and then feature values and time stamps were smoothed using a 50-trial window, gaining the state value.

The continuous modulation index for each feature was averaged among all units within a session to gain the sessions’ mean continuous modulation index. Next, for each session and feature, the continuous index was interpolated, using the ‘interp1’ function with ‘pchip’ as the interpolation method (MATLAB, MathWorks), to gain evenly spaced and mutual values for all sessions. Thereafter, the continuous values were averaged into a grand mean of all sessions of continuous modulation index along the falling asleep (awakening) process (figures 4C-D, 5C).

Rejecting non-significant units

Units with an average spontaneous firing rate <0.5 spikes/sec in any of the vigilance states were excluded from the analysis. Units without a significant response to a single-click stimulus were also excluded from our analysis. The significance of the response was calculated using the Monte Carlo Permutation Test, which was conducted as follows. A unit’s PSTH, in the time interval of [-500ms, 30ms] relative to the beginning of each 2 Hz and 10 Hz Clicks/sec trial, underwent minimal temporal smoothing (gaussian kernel of $\sigma = 2$). The significance was examined separately for the trials before the moment of falling asleep (or awakening) and for the trials after the moment of falling asleep (or awakening). Among the trials of each group, the PSTHs in the baseline interval ([-500ms,0] before click onset) were averaged, as well as the activity in the onset interval ([0, 30ms] after click onset). The difference between the maximum of the averaged PSTH in the time window of the onset and the baseline was calculated. After that, we shuffled between the baselines and the onsets of the smoothed PSTHs (that is, randomly, for 50% of the trials, an exchange was made between the time window of the baseline and the time window of the onset), and then again, we averaged over all the trials, and calculated the difference in the firing rate in the time windows of onset to baseline. This process was performed 1000 times to calculate the surrogate distribution from which the p-value of the real onset response magnitude was derived. Units whose response was not significant, for both before and after falling asleep (or awakening), were also excluded from the analysis.

EEG analysis along arousal state transitions

Frontal EEG signal was extracted around the auditory stimuli within a time window of [-1,1] seconds. Subsequently, for each session, auditory trials occurring during episodes of falling asleep or awakening

were extracted and organized based on their temporal proximity to the moment of falling asleep or awakening. Responses of adjacent trials were smoothed using a moving average window (uniformly weighted) with a size of 100 trials and an overlap of 99 trials. The EEG responses were then stacked according to their relative times, resulting in a raster plot representing the falling asleep or awakening process, as depicted in Fig. 6A (where each row represents an average AEP of 100 temporally-adjacent trials). All trials within the “wakefulness”, “First Seconds of NREM”, and “NREM” periods (-20s < t < -5s, 5s < t < 10s, 60s < t; respectively) were averaged to yield the AEPs in Fig. 6A bottom panels, with the most bottom panel representing the average across all sessions.

Two metrics were calculated from the EEG response. The first, termed the AEP negative deflection metric (Fig. 6B,C, asterisks), was derived from the average AEP response of 100 temporally adjacent trials (Fig. 6B,C). The minimum point within the trough, located in the [50, 150] msec window, was identified, and the integral of the area within the trough was computed. The second metric, baseline (pre-stimulus) slow wave activity (SWA, Fig. 6B,C, diamonds), was calculated as the EEG average Welch’s power spectral density within 0.25-4 Hz frequency range. A running-modulation index was then calculated in relation to the awake period (-20s < t < -5s) showing the temporal dynamics of the auditory cortex post-onset response, auditory cortex population synchrony, EEG AEP negative deflection and the EEG baseline SWA (Fig. 6B,C).

We utilized trial-by-trial variability to explore the relationship between the EEG and neuronal measures (Fig. 6D-I). As before, we temporally sorted all trials relative to the proximate falling asleep (or awakening) episodes. We then took groups of 16 consecutive trials and sorted them to four different groups - Low, Medium Low, Medium High, and High (L, ML, MH, H) - based on their relative post-onset response in the auditory cortex population (i.e. exactly four trials in each group). We then repeated this process for the next 16 trials, and so on, until we sorted all trials into one of these four groups. This process allowed us to create four groups of trials with gradually increasing levels of post-onset response (Fig. 6D left), but with no statistically significant difference in their average timing relative to the proximate falling asleep (or awakening) episode ($p=0.3916$, $n=7$ sessions, Friedman test). We then calculated for each of the four groups of trials the average population synchrony (Fig 6D right), EEG AEP (Fig 6E left), AEP negative deflection magnitude (Fig 6E right), EEG power spectrum (Fig 6F left) and EEG SWA (Fig. 6F right).

In Fig. 6G-I, we performed the same analysis as in Fig. 6D-F described above, but instead of sorting trials based on their relative post-onset response, we instead sorted them based on the relative population synchrony. This (by definition) created four groups of trials with increasing levels of population synchrony (Fig. 6G right), but with no statistically significant difference in their average

timing relative to the proximate falling asleep (or awakening) episode (p=0.7736, n=7 sessions, Friedman test).

Statistics

We used a linear mixed-effects model (LME) to analyze electrophysiological neural data due to its nested and hierarchical nature (Aarts et al., 2014; Makin and De Xivry, 2019). This model was necessary to account for non-independencies in measures from different units obtained in the same electrode, experimental session, or animal. We included animal identity as a random effect, as well as experimental session and microwire electrode as nested random effects within each animal. We obtained model parameters using the 'fitlme' function (Matlab, MathWorks) and utilized restricted maximum likelihood estimation.

When presenting average effects per session, we only considered sessions that had a minimum of 3 units. Throughout the main text, all effect sizes are presented as mean±SEM for all units unless specified otherwise. To evaluate variance across different conditions (>2), we conducted a Friedman test (similar to a non-parametric repeated measures ANOVA) on data summarized at the animal level. This involved averaging all the units for each of the 6 animals. To evaluate differences in EEG activity across two conditions (e.g. comparing wakefulness vs. first-seconds NREM) we conducted a Wilcoxon sign-rank test (WSRT).

Acknowledgments

We thank Dr. Noa Bar-Ilan Regev for administrative assistance. Supported by the Israel Science Foundation (ISF) grants 1326/15 and 1557/22 and by the European Research Council grant ERC-2019-CoG 864353.

Author contributions

A.M. and Y.N. designed the project. A.M. built experimental setup, compiled stimuli, and performed experiments. B.L. led data analysis with support from A.M. and B.H. Y.N. supervised the project and secured funding. All authors wrote the paper.

Declaration of interests

The authors declare that no financial and non-financial competing interests exist.

References

Aarts E, Verhage M, Veenvliet J V., Dolan C V., Van Der Sluis S (2014) A solution to dependency: Using multilevel analysis to accommodate nested data. Nature Neuroscience 17:491–496.

Adamantidis AR, Gutierrez Herrera C, Gent TC (2019) Oscillating circuitries in the sleeping brain. Nature Reviews Neuroscience 20:746–762.

Andrillon T, Poulsen AT, Hansen LK, L É Ger D, Kouider S (2016) Neural markers of responsiveness to the environment in human sleep. Journal of Neuroscience 36:6583–6596.

Atiani S, Elhilali M, David S V., Fritz JB, Shamma S a. (2009) Task Difficulty and Performance Induce Diverse Adaptive Patterns in Gain and Shape of Primary Auditory Cortical Receptive Fields. Neuron 61:467–480.

Barger Z, Frye CG, Liu D, Dan Y, Bouchard KE (2019) Robust, automated sleep scoring by a compact neural network with distributional shift correction. PLoS ONE 14:1–18.

Bergman L, Krom AJ, Sela Y, Marmelshtein A, Hayat H, Regev N, Nir Y (2022) Propofol Anesthesia Concentration Rather Than Abrupt Behavioral Unresponsiveness Linearly Degrades Responses in the Rat Primary Auditory Cortex. Cerebral Cortex.

Eban-Rothschild A, Rothschild G, Giardino WJ, Jones JR, de Lecea L (2016) VTA dopaminergic neurons regulate ethologically relevant sleep–wake behaviors. Nature Neuroscience 19:1–14.

Edeline JM, Dutrieux G, Manunta Y, Hennevin E (2001) Diversity of receptive field changes in auditory cortex during natural sleep. European Journal of Neuroscience 14:1865–1880.

Fukunaga M, Horovitz SG, van Gelderen P, de Zwart JA, Jansma JM, Ikonomidou VN, Chu R, Deckers RHR, Leopold DA, Duyn JH (2006) Large-amplitude, spatially correlated fluctuations in BOLD fMRI signals during extended rest and early sleep stages. Magnetic Resonance Imaging 24:979–992.

Harris KD, Thiele A (2011) Cortical state and attention. Nature Reviews Neuroscience 12:509–523.

Hayat H, Marmelshtein A, Krom AJ, Sela Y, Tankus A, Strauss I, Fahoum F, Fried I, Nir Y (2022) Reduced neural feedback signaling despite robust neuron and gamma auditory responses during human sleep. Nature Neuroscience 25:935–943.

Hori T, Hayashi M, Morikawa T (1994) Topographical EEG changes and the hypnagogic experience.

Issa EB, Wang X (2008) Sensory responses during sleep in primate primary and secondary auditory cortex. J Neurosci 28:14467–14480.

Issa EB, Wang X (2011) Altered neural responses to sounds in primate primary auditory cortex during slow-wave sleep. The Journal of neuroscience : the official journal of the Society for Neuroscience 31:2965–2973.

Issa EB, Wang X (2013) Increased neural correlations in primate auditory cortex during slow-wave sleep. Journal of neurophysiology 109:2732–2738.

Lacaux C, Strauss M, Bekinschtein T, Oudiette D (2023) Embracing sleep onset complexity.

Lee SH, Dan Y (2012) Neuromodulation of Brain States. Neuron 76:109–222.

Linden JF, Liu RC, Sahani M, Schreiner CE, Merzenich MM (2003) Spectrotemporal structure of receptive fields in areas AI and AAF of mouse auditory cortex. Journal of Neurophysiology 90:2660–2675.

Lo CC, Chou T, Penzel T, Scammell TE, Strecker RE, Stanley HE, Ivanov PC (2004) Common scale-invariant patterns of sleep-wake transitions across mammalian species. Proceedings of the National Academy of Sciences of the United States of America 101:17545–17548.

Makin TR, De Xivry JJO (2019) Ten common statistical mistakes to watch out for when writing or reviewing a manuscript. eLife 8.

Marmelshtein A, Eckerling A, Hadad B, Ben-Eliyahu S, Nir Y (2023) Sleep-like changes in neural processing emerge during sleep deprivation in early auditory cortex. Current Biology 33:2925-2940.e6.

Massimini M, Ferrarelli F, Esser SK, Riedner BA, Huber R, Murphy M, Peterson MJ, Tononi G (2007) Triggering sleep slow waves by transcranial magnetic stimulation. Proceedings of the National Academy of Sciences of the United States of America 104:8496–8501.

Massimini M, Ferrarelli F, Huber R, Esser SK, Singh H, Tononi G (2005) Breakdown of cortical effective connectivity during sleep. Science 309:2228–2232.

Mcginley MJ, Vinck M, Reimer J, Batista-brito R, Zagha E, Cadwell CR, Tolias AS, Cardin JA, Mccormick DA (2015) Waking State : Rapid Variations Modulate Neural and Behavioral Responses. Neuron 87:1143–1161.

Nir Y, de Lecea L (2023) Sleep and vigilance states: Embracing spatiotemporal dynamics. Neuron 111:1998–2011.

Nir Y, Vyazovskiy V V, Cirelli C, Banks MI, Tononi G (2013) Auditory Responses and Stimulus-Specific Adaptation in Rat Auditory Cortex are Preserved Across NREM and REM Sleep. Cerebral cortex (New York, NY : 1991):bht328-.

Nir Y, Vyazovskiy V V., Cirelli C, Banks MI, Tononi G (2015) Auditory Responses and Stimulus-Specific Adaptation in Rat Auditory Cortex are Preserved Across NREM and REM Sleep. Cerebral Cortex 25:1362–1378.

Ogilvie RD (2001) The process of falling asleep. Sleep Medicine Reviews 5:247–270.

Okun M, Steinmetz NA, Cossell L, Iacaruso MF, Ko H, Barthó P, Moore T, Hofer SB, Mrsic-Flogel TD, Carandini M, Harris KD (2015) Diverse coupling of neurons to populations in sensory cortex. Nature 521:511–515.

Paxinos G, Watson C (2006) The rat brain in stereotaxic coordinates: hard cover edition. Elsevier.

Pigorini A, Sarasso S, Proserpio P, Szymanski C, Arnulfo G, Casarotto S, Fecchio M, Rosanova M, Mariotti M, Lo Russo G, Palva JM, Nobili L, Massimini M (2015) Bistability breaks-off deterministic responses to intracortical stimulation during non-REM sleep. NeuroImage 112:105–113.

Quiroga RQ, Nadasdy Z, Ben-Shaul Y (2004) Unsupervised spike detection and sorting with wavelets and superparamagnetic clustering. Neural computation 16:1661–1687.

Rodriguez XA V, Funk XCM, Vyazovskiy XV V, Nir XY, Tononi G, Cirelli XC (2016) Why Does Sleep Slow-Wave Activity Increase After Extended Wake ? Assessing the Effects of Increased Cortical Firing During Wake and Sleep. 36:12436–12447.

Sela Y, Krom AJ, Bergman L, Regev N, Nir Y (2020a) Sleep differentially affects early and late neuronal responses to sounds in auditory and perirhinal cortices. Journal of Neuroscience 40:2895–2905.

Sela Y, Krom AJ, Bergman L, Regev N, Nir Y (2020b) Sleep Differentially Affects Early and Late Neuronal Responses to Sounds in Auditory and Perirhinal Cortices. The Journal of Neuroscience 40:2895–2905.

Sela Y, Vyazovskiy V V., Cirelli C, Tononi G, Nir Y (2016) Responses in rat core auditory cortex are preserved during sleep spindle oscillations. Sleep 39:1069–1082.

Strauss M, Sitt JD, King JR, Elbaz M, Azizi L, Buiatti M, Naccache L, Van Wassenhove V, Dehaene S (2015) Disruption of hierarchical predictive coding during sleep. Proceedings of the National Academy of Sciences of the United States of America 112:E1353–E1362.

Strauss M, Sitt JD, Naccache L, Raimondo F (2022) Predicting the loss of responsiveness when falling asleep in humans. NeuroImage 251.

Vyazovskiy V V., Olcese U, Cirelli C, Tononi G (2013) Prolonged wakefulness alters neuronal responsiveness to local electrical stimulation of the neocortex in awake rats. Journal of Sleep Research 22:239–250.

Vyazovskiy V V, Olcese U, Hanlon EC, Nir Y, Cirelli C, Tononi G (2011) Local sleep in awake rats. Nature 472:443–447.

Vyazovskiy V V., Olcese U, Lazimy YM, Faraguna U, Esser SK, Williams JC, Cirelli C, Tononi G (2009) Cortical Firing and Sleep Homeostasis. Neuron 63:865–878 Available at: http://dx.doi.org/10.1016/j.neuron.2009.08.024%5Cnhttp://www.ncbi.nlm.nih.gov/pubmed/19778514.

Xu Y, Wokke M, Noreika V, Bareham C, Jagannathan S, Georgieva S, Trentin C, Bekinschtein T (2023) Effects of alertness on perceptual detection and discrimination. bioRxiv:2023.03.21.533623.